Accepted Manuscript

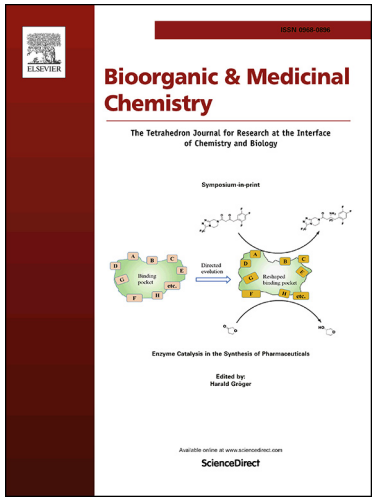

Design, synthesis and QSAR study of 2′-hydroxy-4′-alkoxy chalcone derivatives that exert cytotoxic activity by the mitochondrial apoptotic pathway

Silvia Marquina, Maritza Maldonado-Santiago, Jessica Nayelli Sánchez-Carranza, Mayra Antúnez-Mojica, Leticia González-Maya, Rodrigo Said Razo-Hernández, Laura Alvarez

PII: S0968-0896(18)31437-8
DOI: https://doi.org/10.1016/j.bmc.2018.10.045
Reference: BMC 14604

To appear in: *Bioorganic & Medicinal Chemistry*

Received Date: 21 August 2018
Revised Date: 17 October 2018
Accepted Date: 30 October 2018

Please cite this article as: Marquina, S., Maldonado-Santiago, M., Nayelli Sánchez-Carranza, J., Antúnez-Mojica, M., González-Maya, L., Said Razo-Hernández, R., Alvarez, L., Design, synthesis and QSAR study of 2′-hydroxy-4′-alkoxy chalcone derivatives that exert cytotoxic activity by the mitochondrial apoptotic pathway, *Bioorganic & Medicinal Chemistry* (2018), doi: https://doi.org/10.1016/j.bmc.2018.10.045

Design, synthesis and QSAR study of 2′-hydroxy-4′-alkoxy chalcone derivatives that exert cytotoxic activity by the mitochondrial apoptotic pathway

Silvia Marquina[1], Maritza Maldonado-Santiago[1], Jessica Nayelli Sánchez-Carranza[2], Mayra Antúnez-Mojica[1], Leticia González-Maya[2], Rodrigo Said Razo-Hernández[3], Laura Alvarez[1*]

[1]Centro de Investigaciones Químicas-IICBA, [2]Facultad de Farmacia, [3]Centro de Investigación en Dinámica Celular-IICBA. Universidad Autónoma del Estado de Morelos, Avenida Universidad 1001, Chamilpa, Cuernavaca, Morelos 62209, México. smarquina@uaem.mx; maritza.maldonados@uaem.edu.mx; jes_chazaq@hotmail.com; myam@uaem.mx; letymaya@uaem.mx; rodrigo.razo@uaem.mx; lalvarez@uaem.mx

Corresponding author
Dra. Laura Alvarez
Centro de Investigaciones Químicas-IICBA
Universidad Autónoma del Estado de Morelos (UAEM)
Av. Universidad 1001, Col. Chamilpa, Cuernavaca, Morelos 62209, México
Tel: +52 777 3297997
lalvarez@uaem.mx

Abstract

Eleven 4′-alkoxy chalcones were synthesized and biologically evaluated for their antiproliferative activity against four human tumor cell lines (PC-3, MCF-7, HF-6, and CaSki). Compounds **3a-3d** and **3f** were selective against PC-3, with IC_{50} values ranging from 8.08 to 13.75 μM. In addition, chalcones **3a-3c** did not affect the normal fibroblasts BJ cells. The most active and selective compounds were further evaluated for their effect on the progression of cell cycle in PC-3 cells, and chalcones **3a** and **3c** induced a G2/M phase arrest. Furthermore, it was found that these three chalcones induced the mitochondrial apoptotic pathway by regulating Bax and Bcl-2 transcripts and by increasing caspase 3/7 activation. Otherwise, the QSAR model indicates that the double bond of the α,β-unsaturated carbonyl, as well as the planar structure geometry, are important to the biological activity of the synthetized chalcones. Based on these studies, it was concluded that withdrawing substituents in ring A, decrease the antiproliferative activity. This is related to the possible mechanism of action of these compounds, where a Michael addition needs to take place in order to be a potent anticancer agent.

Keywords: Chalcones, antiproliferative activity, QSAR study, cell cycle, apoptosis, Bax/Bcl-2, caspase 3/7, cancer.

1. Introduction

Chalcones (1,3-diaryl-2-propen-1-ones) are natural open chain flavonoids widely biosynthesized in plants.[1] Structurally, they consist of two aryl groups (A- and B-rings) connected by an α, β-unsaturated ketone moiety that typically assumes the thermodynamically more stable *E* configuration. Scientific research has demonstrated that chalcones display a variety of interesting biological activities such as antioxidant, cytotoxic, anticancer, antimicrobial, antiviral, antiprotozoal, antiulcer, antihistaminic and anti-inflammatory.[2,3] As for antitumor activity, chalcones exhibit various effects including anti-initiation, apoptosis induction, antiproliferation, antimetastasis, antiangiogenesis, DNA and mitochondrial damage, tubulin inhibition and so forth.[4,5]

Because of their structural simplicity and the associated ease of synthesis, chalcones continue to enjoy considerable attention from medicinal chemists exploring new molecular scaffolds for the novel therapeutics design.[6,7]

Among the naturally occurring hydroxy chalcones, 2′,4′-dihydroxychalcone (2,4DHC; **3a**), which is a flavonoid isolated from various medicinal plants, [8,9] displays antibacterial and antifungal properties.[10] Also, this compound has been proved to be antigenotoxic on HepG2 cells.[11] Experimental studies have shown the antiproliferative activity of 2,4DHC on cancer cells.[12,13] Further, it has been demonstrated that induce apoptosis on human gastric cancer cells,[14] and damage to the DNA which results in a Rad3-dependent and Chk1-dependent cell cycle and block at the G2/M transition.[15]

Inspired in the chemical structure of 2,4DHC (**3a**), and in an effort to discover more effective compounds, here, we synthesized 2′-hydroxy, 4′-alkoxy-chalcone derivatives (**3a-k)** and were evaluated for their antiproliferative activity against a panel of four human cancer cell lines including MCF-7 (breast), HF-6 (colon), CaSki (cervical), and PC-3 (prostate). Among all the compounds, chalcones **3a-c** displayed the most potent antitumor activity against the PC-3 cancer cell line and were choose for determine their capacity to cause cell cycle arrest and to induce apoptosis. In addition, the antiproliferative properties of these molecules were evaluated by a quantitative structure activity relationship study (QSAR), employing global and local chemical reactivity molecular descriptors such as:

chemical hardness (η), softness (S), chemical potential (μ), Electrophilicity (ω) and Fukui function.

2. Results and discussion

2.1. Synthesis

In this study we synthesized eleven derivatives of 2′,4′-dihydroxychalcone (**3a**), to try to potentiate its cytotoxic effects. In comparison with the parttern structure **3a**, we inserted different substituents in C-4′, such as methyl, ethyl, propyl, benzyl and acetate, as well as halogens in C-3′ and C-5′, leaving intact B ring. It is important to mention that there are few reports about this type of chalcones.

Alcoxyacetophenones (**2b-e**) were obtained by alkylation of 2,4-dihydroxy acetophenone with methyl iodine, bromoethane, bromopropane, and benzyl bromide, respectively, in the presence of K_2CO_3. The 2-hydroxy-4-acetylacetophenone (**2f**) was prepared by acylation of **2a** with acetic anhydride and pyridine. Otherwise, chalcones were prepared by Claisen-Schmidt condensation of the appropriate 2-hydroxy-4-alkoxy-acetophenone (**2b-2f**) with benzaldehyde (**1**) in the presence of KOH. 2′,4′-dihydroxy chalcone (**3a**) was prepared through demethylation with BBr_3 of the corresponding 4′-methoxy derivative chalcone (**3e**). Substitution pattern on A-ring was changed adding Br and I atoms at C-3’ and C-5’ (derivatives **3g-j**). Finally, catalytic hydrogenation of **3b** afforded the dihydroderivative **3k**. Chalcone derivatives were characterized by 1D NMR and mass spectra analysis. The general procedures for the synthesis of chalcone derivatives are described in Scheme 1.

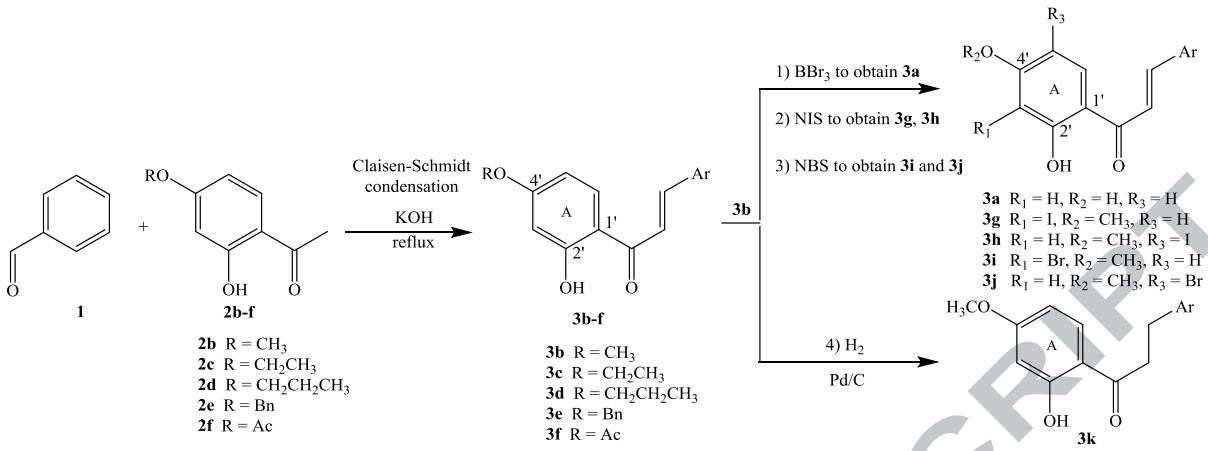

Scheme 1. Synthesis of chalcones **3a-3k**.

2.2. Biological Activity

The synthesized chalcones (**3a-3k**) with purity values over 95% were evaluated by the MTT assay for their capacity to inhibit the *in vitro* growth of breast (MCF-7), colon (HF-6), cervical (CaSki), and prostate (PC-3) human cancer cell lines. We also included human fibroblasts cell line (BJ) as a control of non-cancerous cells. Results are summarized in Table 1 which indicate that chalcones displayed selectivity against PC-3 cell line, where the derivatives 2′,4′-dihydroxychalcone (**3a**), 2′-hydroxy-4′-methoxychalcone (**3b**), 4′-ethoxy-2′-hydroxy-chalcone (**3c**), 2′-hydroxy-4′-propoxychalcone (**3d**) and 4′-acetoxy-2′-hydroxy-chalcone (**3f**) were the most potent with IC_{50} values of 13.75, 11.81, 8.2, 8.08, and 10.035 μM, respectively. In addition, compounds **3a**, **3b** and **3c** were selective to cancer cells, unlike **3d** and **3f** that were cytotoxic also against human fibroblast cells.

Table 1. Antiproliferative activity (IC_{50} values) of synthetic chalcones **3a-k** against four human tumor cell lines and one no tumoral (BJ).

Compound	**IC_{50} (Mean ± S.D., μM)**				
	BJ	**PC-3**	**MCF-7**	**HF-6**	**CaSki**
3a	262.5±8	13.75±0.35	> 50	ND	ND
3b	239.17±7	11.81±0.25	> 50	> 50	ND
3c	207.87±7	8.2±0.15	> 50	ND	ND
3d	15.95±2.5	8.08±0.032	> 50	ND	> 50
3e	ND	34.66±0.18	> 50	ND	> 50
3f	21.27±3.5	10.035±0.21	> 50	> 50	> 50
3g	ND	34.037±0.5	> 50	> 50	> 50
3h	ND	> 50	> 50	> 50	> 50
3i	ND	47.78±0.45	> 50	> 50	> 50
3j	ND	> 50	> 50	38.90±0.02	> 50

3k	ND	> 50>	> 50	> 50	> 50
PDX	5.0±0.35	0.12±0.027	0.28±0.026	0.0369±0.014	0.3±0.003

ND = no determined PDX = Podophyllotoxin (positive control)

Similar studies reported that the structurally related 2,2′,-dihydroxychalcone caused growth inhibition in four cell lines, showing to be more effective in the prostate cancer cell line (IC_{50} = 10.26 μM).[16]

By the other hand, a series of 2′,4′-dihydroxychalcones possessing both halogen and methoxyl groups on B ring and hydroxyl and alkyl groups on A ring were investigated for their ability to inhibit *in vitro* growth of three human tumor cell lines, MCF-7 (breast adenocarcinoma), NCI-H460 (non-small cell lung cancer) and A375-C5 (melanoma). The results showed that 3,4,5-trimethoxy-2′,4′-dihydroxychalcone and 4-fluoro-2′,4′-dihydroxychalcone were the most active against MCF-7 cell line with IC_{50} values of 7.8 ± 0.5 and 7.3 ± 0.6 μM respectively.[17]

2.3. Cell Cycle analysis

Several studies have shown that the antiproliferative activity of chalcones is due to their interference with different cell cycle phases. Previous studies with chalcone derivatives have demonstrated that many of these compounds cause arrest in G2/M phase.[16,18,19] Some chalcones may bind to tubulin, preventing polymerization of the microtubule and therefore causing blocking in the G2/M phase of the cell cycle of K562 and Jurkat cells.[20-22]

This information agrees with our results, we examined the effect of the synthesized chalcones (**3a-3c**) in the cell cycle progression of PC3 cancer cells, using the IC_{50} values previously determined. Figure 1 displays DNA histograms of PC3 cells treated in the presence of **3a-3c** and controls. One of the changes more frequently observed in the cell cycle of PC3 cancer cells is the G2/M phase arrest. For instance, compound **3a** (13.75 μM) induced a G2/M phase arrest in PC3 cells by increasing from 24.9 % to 40.8 % with respect to the negative control (Figure 1B), while **3c** (8.2 μM) to 50.1% (Figure 1D) and chalcone **3b** at 11.81 μM the increase in G2/M was not significant (27.1 %) (Figure 1C).

In addition, in this study, chalcones **3a**-**3c** significantly increased the subG1 phase population, this suggests DNA damage, cell death or cellular senescence (Figures 1B-1D).

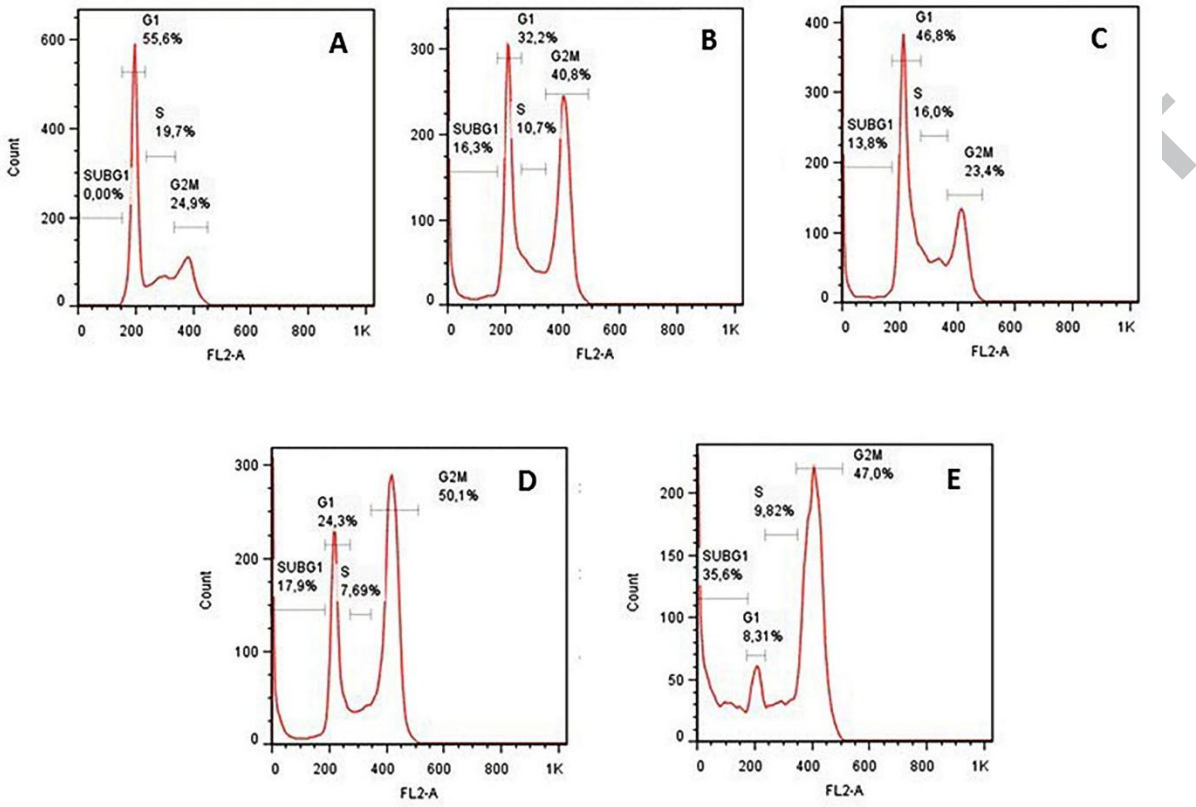

Fig. 1. Effect of chalcones on cell cycle in PC3 cell line of prostate cancer. A) Negative Control; B) **3a**; C) **3b**; D) **3c**; E) Podophyllotoxin (positive control).

2.4. Cell death

Several studies have reported that chalcones can block the cell cycle in the G2/M phase,[21] while others show blocking in the G0/G1 phase.[23,24] However, the effect of chalcones and their derivatives in the transduction of signals which control the cell cycle and induce apoptosis of cells are still controversial. To elucidate the type of cell death induced by compounds **3a-3c** in PC3 cells, we investigated whether these compounds could induce apoptosis. PC3 cells treated with compound **3a, 3b** and **3c**, according to their IC_{50}, were observed by fluorescence microscopy of orange-ethidium acridine bromide clear condensation of chromatin, plasma membrane blistering and apoptotic bodies formation were observed; similar morphological changes were observed when apoptosis was induced by the positive controls H_2O_2 (Figure 2F) and podophyllotoxin (Figure 2G).

It was also observed the chromatin condensation and yellow-green nuclei (white arrows) in the presence of all compounds (Figures 2C-2E), while membrane invaginations are clearly seen in the effect caused by compound **3c**; Figure 2E presents the morphological changes such as chromatin condensation, plasma membrane blebbing and formation of apoptotic bodies. Our results in the increase of SubG1 phase were correlated with the morphological changes observed which are characteristic of apoptosis. These results are in agreement with the increase of the subG1 population previously observed in the cell cycle histograms showed in **Figure 1**.

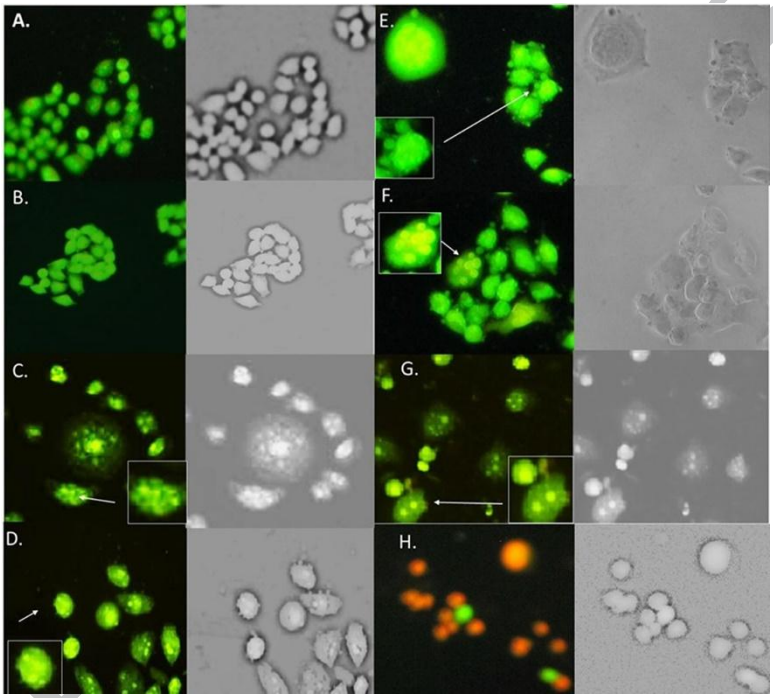

Fig. 2. Effect of chalcones on cell death by epifluorescence microscopy in PC3 cell line of prostate cancer. A) andB) Negative Controls; C) **3a**; D) **3b**; E) **3c**; F) H_2O_2 apoptosis positive control; G) Podophyllotoxin 0.005 µM apoptosis positive control; H) Necrosis control.

*2.4.1. Apoptosis characterization: Evaluation of the effect of chalcones **3a-c** on the expression of Bax, Bcl-2 and caspases 3/7 activation in PC-3 cell line*

Apoptotic pathway has been described as an important signaling of cell death for mammalian cells.[25] It is well documented that activating caspase-9, cause the activation of effector caspases (-3, -6 and -7) in the apoptosis of intrinsic pathway; also an increase of the pro-apoptotic Bax expression and down-regulation of the anti-apoptotic Bcl-2[26,27] is observed. The ratio of Bax/Bcl-2 is critical for the apoptosis induction by the mitochondrial pathway.[28,29] It has been described in the literature some studies showing that chalcones

induce cell death via apoptotic pathways, for instance, the K562 cells treated with a synthetic chalcone induced apoptosis through the mitochondrial pathway and activated caspase-3, while Jurkat cells can reduce the expression of the anti-apoptotic gene Bcl-2 and increase the expression of the pro-apoptotic gene.[20,30]

This motivated us to look at the effect of the **3a-3c** chalcones on the levels of Bax/Bcl-2 and caspase3/7 activation on PC3 cells. The results showed that compounds, **3a-3c** clearly inhibited Bcl-2 and increased Bax transcripts in PC3 cells (Figure 3) and showed a clear increase in caspase 3/7 activation statistically significant as compared to the control (Figure 4) suggesting that **3a-3c** cause cell death by mitochondrial apoptotic pathway.

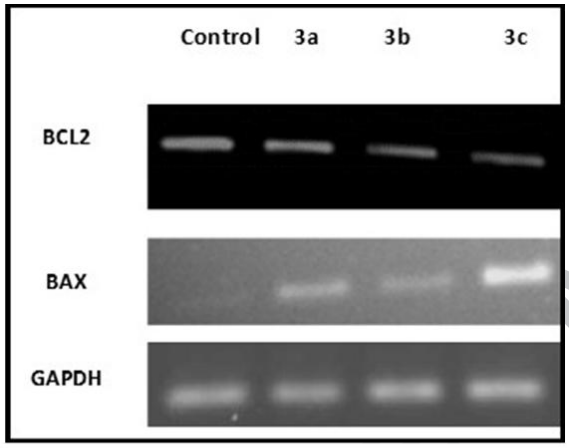

Fig. 3. Effect of **3a**, **3b** and **3c**, on mRNA expression levels of Bcl-2 and Bax in PC3 cells after 48 hours treatment. GAPDH was used as an internal control.

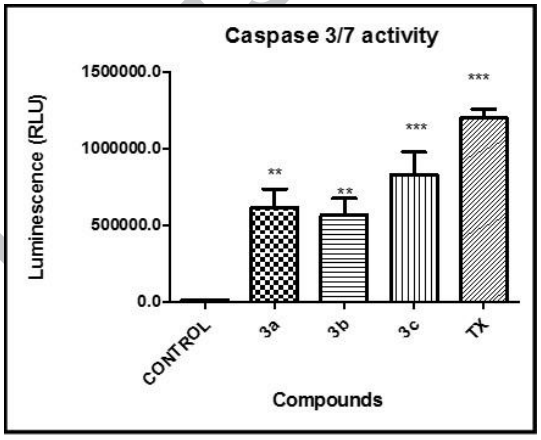

Fig. 4. Caspase 3/7 activity for treatment of **3a**, **3b**, **3c**, and paclitaxel (TX) in PC3 cells. *p<0.05, **p<0.01, ***p<0.001 compared with the control group

2.6. Computational results

2.6.1. Geometry optimization and Molecular Graphics

From the conformational analysis of all the chalcone derivatives (**3a-3k**) and their subsequent optimization geometry, the minimum energy structure of all the chalcones was obtained, since all their frequencies were positive. The optimized structure of all the chalcone derivatives was obtained, and the LUMO and ionization potential maps, are displayed in Figures 5 and 6 respectively.

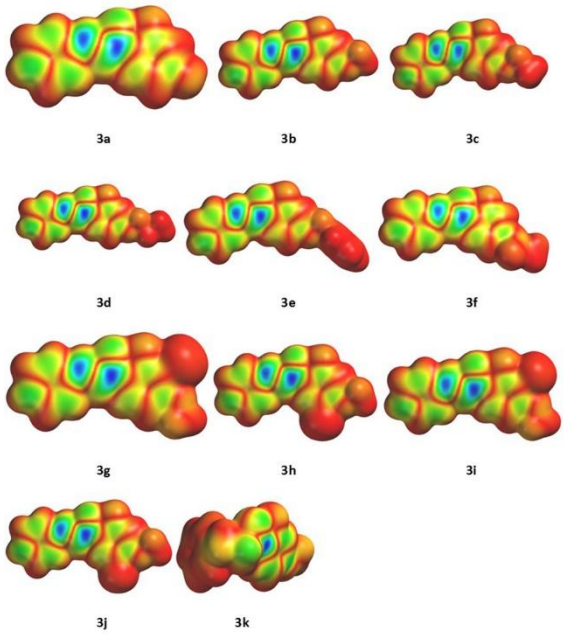

Fig. 5. LUMO map of all the chalcone derivatives (**3a**-**3k**). Blue, green, yellow and red colors indicate the most, medium, poor and none populated region of the LUMO orbital, respectively.

It can be noted that almost all the chalcones share a similar plane structure geometry, regardless molecule **3k**. This fact is related to its lack of double bound between the phenyl ring and the carbonyl moiety. From the LUMO map analysis we can see how this lack of double bond in the chalcone skeleton affects its electronic distribution (Figure 5). The rest of the chalcones had their LUMO map with similar characteristics; LUMO map indicated the regions of a molecule that are most sensitive to nucleophilic attack (blue color regions). One region is on the carbonyl carbon, and the other region is on the β carbon; like in a simple α,β-unsaturated carbonyl compound. This fact may explain why molecule **3k** has not anticancer activity. Nevertheless, molecules **3j** and **3h** possess the same LUMO map characteristics of the biological active chalcones and they are inactive. That is why we employed the potential ionization map to identify the molecule zones that are more prone to suffer an electrophilic attack (red zones, Figure 6).

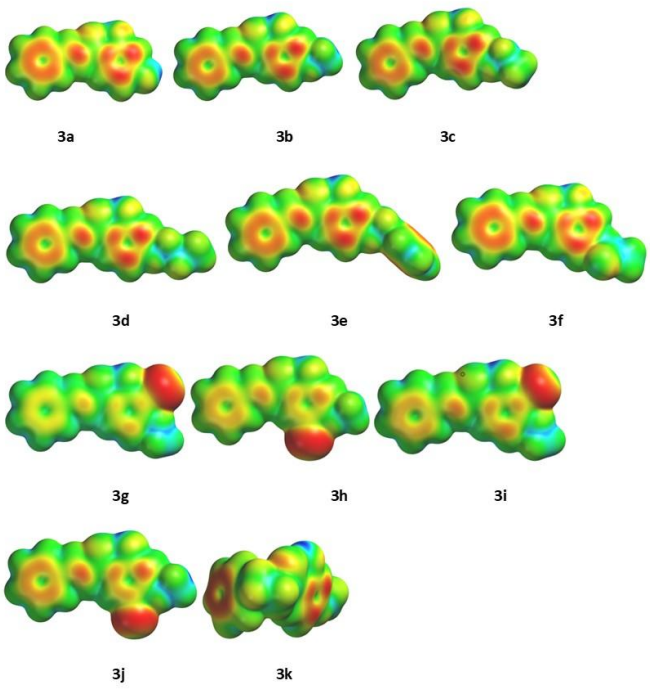

Fig. 6. Local ionization potential map of all the chalcone derivatives (**3a-3k**). Red, yellow, green and blue colors indicate zones from which electrons are most easily, medium, less and unlikely ionized, respectively.

From Figure 6 we can observe that the substitution of an halogen atom in the benzene ring affects its local ionization potential, like in **3g**, **3h**, **3i** and **3j**. In addition, a decrease in the ionization potential occurs in the region of the double bond where the Cα and Cβ are located. This may explain the low and lack of biological activity of the molecules that possess one halogen atom in their benzene ring (**3g-3j**). From these results, we can deduce that electron withdrawing substituents in ring A affects the biological activity of the chalcones, specially substitutions in the C-5′ of ring A, since they losses their anticancer biological activity.

Analyzing the values of the global reactivity molecular descriptors (Table S1) it can be observed that **3k** has the greater chemical hardness value, this can be caused by its lack in the double bond between the ring B and the carbonyl group and this fact may explain its biological inactivity. Contrary to **3h** and **3j** that have the lowest values of chemical hardness, therefore **3h** and **3j** are the softest molecules. These molecules for our study were biologically inactive, we cannot attribute this to the presence of halogen atoms in their

structure (Br and I) because **3g** and **3i** also have them. Therefore, the location of halogen atoms in ring A is crucial for their anticancer activity, this can be related to the resonance and inductive effects related to the position were the substitution occurred. It is worthy of mention the works of Fortuna et al, who used the Volsurf approach to design and synthesized several new halogenated heterocyclic compounds with potent antiproliferative activity against different cell lines, especially MCF-7.[31, 32]

2.6.4. QSAR study

On the other hand, from the molecular graphics results we can observe that the carbonyl and substituted benzene of the chalcones are key for their biological activity. Nevertheless, we still cannot explain the differences in IC_{50} between the active chalcones. For this reason and considering the small number of molecules, we performed a QSAR study employing global and local reactivity chemical quantum descriptors of the chalcones; QSAR models of a small number of compounds have been successfully used to help explaining their biological activity. The best mathematical model according to all the statistical parameters is shown below.

$$IC_{50} = 1591.42518[f_{C\alpha}^{-}] + 4419.50362[f_{C\beta}^{-}] \mp 156.96115 \quad (1)$$

$$R^2 = 90.38 \qquad Q^2_{LOO} = 79.03 \qquad s = 5.64 \qquad F = 23.3$$

$$\Delta K = 0.40\ (0.0)\ \Delta Q = 0.04(-0.005)\ \ R^p = 0.15(0.10)\ \ R^N = -0.19(-0.49)$$

Because of the small number of compounds in this study, the number of descriptors allowed in the QSAR model is very low. Therefore, to ensure a non-collinearity between descriptors the QUIK rule had to be approved ($\Delta K = 0.40$). In the same manner to avoid a QSAR model with an excess of good or bad descriptors the redundancy ($R^p = 0.16$) and overfitting ($R^N = -0.18$) rules were checked. Additionally, to have a greater guarantee of the QSAR model predictive ability we used the Asymptotic Q^2 rule ($\Delta Q = 0.04$) as a determinant for the model selection. QSAR model indicates that the double bond of the α,β-unsaturated carbonyl is directly correlated to the biological activity of the chalcones. The f^- of the Cα and Cβ are the molecular descriptors that helps us to describe how the chemical reactivity of the chalcones affects their anticancer activity. This equation agrees with the LUMO and potential ionization maps described before. According to the QSAR

equation, if we increase the negative value of f^- of Cα and Cβ atoms, the biological activity of the chalcones will increment (Table 2).

Table 2. Values of the molecular descriptors present in the QSAR model and the biological activity (IC_{50}) of chalcones.

Molecule	$f_{C\alpha}^-$	$f_{C\beta}^-$	IC_{50} (μM)
3a	-0.025	-0.025	13.75
3b	-0.021	-0.025	11.81
3c	-0.018	-0.027	8.2
3d	-0.019	-0.025	8.84
3e	-0.017	-0.023	34.67
3f	-0.027	-0.023	10.04
3g	-0.019	-0.018	47.79
3h	-0.01	-0.023	> 50
3i	-0.023	-0.019	34.04
3j	-0.008	-0.019	> 50
3k	0.016	0.013	> 50

Since we do not possess an exact quantitative IC_{50} value for the **3f**, **3h**, and **3j** molecules, they were not considered for the construction of the QSAR model. All the experimental biological activity (Y_{exp}), the calculated and predicted biological activities (Y_{cal} and Y_{pred}) by the QSAR model and leverage values (Hat) of chalcones are presented in Table 3. Also, the Calculation Error and Prediction Error values which states for the differences between Y_{exp} and both Y_{cal} and Y_{pred}, are presented by the $residual_{cal}$ and the $residual_{pred}$ terms respectively.

Table 3. Values of the anticancer experimental Y_{exp}, calculated Y_{cal} and predicted Y_{pred} activities, and $residual_{\text{cal}}$ and $residual_{\text{pred}}$ values are shown.

Molecule	Y_{exp}	Y_{cal}	Y_{pred}	Hat	$residual_{\text{cal}}$	$residual_{\text{pred}}$
3a	13.75	6.69	2.7	0.361	-7.06	-11.05
3b	11.81	13.05	13.32	0.18	1.24	1.51
3c	8.2	8.99	9.59	0.431	0.79	1.39
3d	8.84	16.24	18.32	0.22	7.4	9.48
3e	34.67	28.26	25.26	0.40	-6.41	-9.41
3f	10.04	12.34	14.79	0.51	2.31	4.75
3g	47.79	47.17	46.32	0.58	-0.62	-1.47
3h	> 50	-	-	-	-	-
3i	34.04	36.39	37.94	0.31	2.35	3.9
3j	> 50	-	-	-	-	-
3k	> 50	-	-	-	-	-

The linear relation of Y_{exp} versus Y_{cal} plot is shown in Figure 7A, Y_{cal} values are obtained using the QSAR model. The squared correlation coefficient (R^2) of the QSAR, which explain the variance of the description model, is shown. From this figure it can be noted that the mathematical model possesses a respectable descriptive ability taking into account the small number of molecules, even the low values of the biological activity are well approximated. Also, linear relation of the Y_{exp} versus Y_{pred} plot is shown in Figure 7B, Y_{pred} values are obtained employing the leave one out technique. The squared correlation coefficient (R^2) corresponds to the value of the explained variance in prediction of the QSAR model $Q^2_{LOO} = 79.03$.

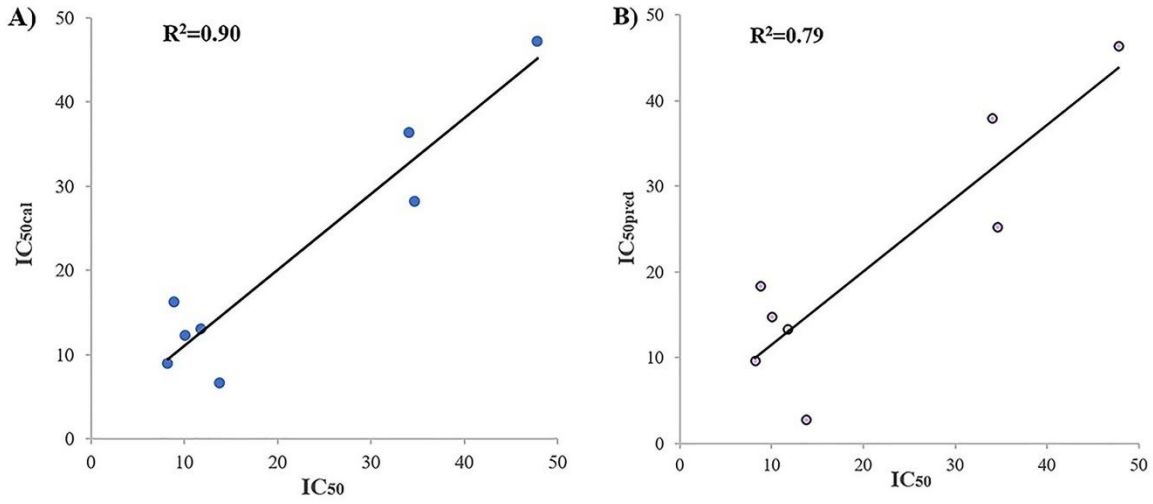

Fig. 7. A) Linear relation of calculated activity versus experimental activity. B) Linear relation of predicted activity versus experimental activity.

William plot based on the prediction residuals and the leverage values was used to define the applicability domain of the chalcones anticancer activity prediction model (Figure 8). From William plot, both structural outside compounds ($h > h^*$) and response outliers ($residual_{pred} > 3SDEC$) can be detected.

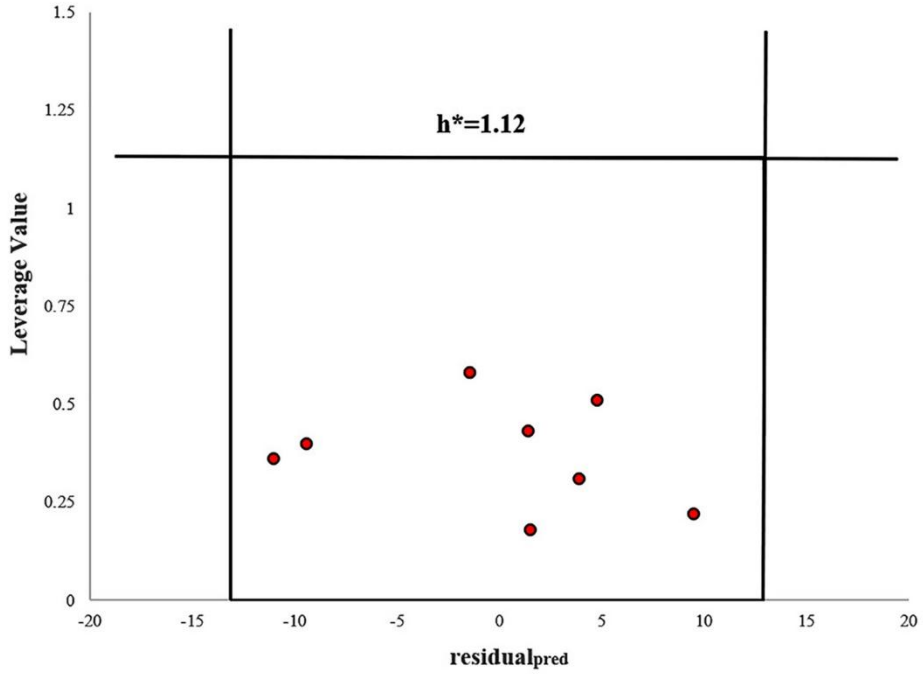

Fig. 8. Williams plot of prediction residuals versus leverage values of chalcones. The horizontal line shows the warning leverage ($h^* = 3p/n$, n is the number of chalcones and p is the number of descriptors in the model plus one), the two vertical lines indicate the bounds within which all of residuals should lie (3SDEC=13.38).

Compounds outside the area formed by the three black lines are identified as outliers. These lines represent the warning leverage (h*, horizontal line) and three times the standard deviation in calculation error (SDCE, vertical lines). All the chalcones fell within the applicability domain of the model, suggesting the application of this model for the prediction of the anticancer activity of new chalcones with high structure similarity.

From these Figures it can be shown that the QSAR model calculates in a good proportion the IC_{50} experimental values, with an exception for **3a** and **3e**. Where their calculation is complicated since **3a** has the same value of f^- for Cα and Cβ, and **3e** possesses a low value of f^- for Cα.

QSAR equation shows that $f_{C\beta}^-$ is the descriptor with major importance for the biological activity of chalcones (higher coefficient value). This can be explained by the chemical mechanism that these compounds (α,β-unsaturated carbonyl) may suffer. Since

f_A^- represents the Fukui function in terms of the removal of an electron from the molecule, and more specific, the effect of removing one electron from atom A. If we have values of $f_{C\beta}^-$ that are higher than those of $f_{C\alpha}^-$, this will indicate that a Michael addition is taking place rather than a carbonyl addition. Implying that chalcones undergoing a Michael addition will possess higher anticancer activity that those undergoing a carbonyl addition.

Analyzing the molecular graphics and QSAR results it can be deduced that the incorporation of electron withdrawing groups in ring A, reduces the anticancer activity of chalcones over the PC-3 cell line. These electron withdrawing groups trigger a nucleophilic attack over the carbon of the carbonyl group; facilitating that a carbonyl addition takes place. This is related to the possible mechanism of action of these compounds, where a Michael addition needs to take place so that the chalcones can have a potent anticancer activity. Additionally, this hypothesis is supported by the fact that molecule **3k,** which lacks a double bond between ring B and the carbonyl moiety, did not display anticancer activity. Corroborating the importance of the double bond for the activity of these molecules, which fits perfectly with our QSAR model. Where these chalcones undergoes a covalent mechanism to be active as anticancer compounds, reacting with a protein (with their serine and threonine residues) or nucleic acid (phosphate groups) important for the cell stability.

3. Conclusions

In this study, derivatives of 2′-hydroxy-4′-alkoxy chalcones (**3a**-**k**) were selected and synthesized from different side chains at position 4′ of ring A and leaving ring B without substituents. Antiproliferative assay revealed that the synthetized compounds displayed selective cytotoxicity against PC-3 cell line, and three compounds **3a**-**3c** showed the highest activity. Further studies on the mechanism demonstrated that these three chalcones induced the mitochondrial apoptotic pathway by regulating Bax and Bcl-2 transcripts and by increasing caspases 3/7 activation. In addition, chalcones **3a** and **3c** induced a G2/M phase arrest. Finally, QSAR study suggested the importance of the α,β-unsaturated ketone and the planar structure geometry for the biological activity, in which, electron withdrawing substituents in ring A decrease the anticancer activity of chalcones, by switching its reactivity so that a carbonyl addition occurs rather than a Michael addition.

The combined *in vitro* effects suggest that chalcones **3a**-**3c** are compounds with bioactive potential that might be used as lead compounds for the development of antitumoral drugs in the coming future.

4. Experimental section

4.1. General procedure: Chemistry

All commercial regents: 2,4-dihydroxyacetophenone (99%), benzaldehyde (99.5%), iodomethane (99%), bromoethane (98%), bromopropane (99%) and benzyl bromide (98%), were obtained from Sigma-Aldrich and were used without further purification. Melting points where determined in a Fisher Johns and are uncorrected. NMR spectra were recorder with a Varian System instrument (400 MHz for ^{1}H, and 100 MHz for ^{13}C), employing $CDCl_3$ as solvent and TMS as internal reference; chemical shifts (δ) are expressed as ppm and coupling constants (*J*) in Hertz. Multiplicities are indicated as singlet (s), doublet (d), triplet (t), quartet (q), double of double (dd), multiplet (m) and broad singlet (bs). Open column chromatographies were carried out on silica gel 60 (70–230 and 230–400 mesh), different solvent systems as mobile phase was used for the purification (*n*-hexane and EtOAc). Mass spectra were obtained in a Joel M-station JEOL JMX-AX 505 HA mass spectrometer.

*4.2. Synthesis of 2'-hydroxy-4'-alkoxy-acetophenones **2a**-**2f***

2'-hydroxy-4'-alkoxy-acetophenones **2b**-**2e** were obtained separately by alkylation with 2,4-dihydroxy acetophenone (**2a**) (1 g, 6.58 mmol) in presence of each halide; iodomethane (1.23 mL, 19.74 mmol), bromoethane (1.47 mL, 19.74 mmol), bromopropane (1.69 mL, 19.74 mmol) and benzyl bromide (0.39 mL, 3.28 mmol) respectively, using K_2CO_3 (0.91 g, 6.58 mmol) as a base, in acetone (10 mL). Each reaction mixture was heated at reflux for 13 h. The crude reactions were purified separately by column chromatography on silica gel eluting with 98:02 *n*-hexane-EtOAc This procedure afforded **2b** (720 mg, 65.9%), **2c** (870 mg, 73.5%), **2d** (950 mg, 74%), and **2e** (370 mg, 23.2%). **2f** was prepared by acetylation of **2a** (1g, 6.58 mmol) with acetic anhydride/pyridine 2:1. The crude reaction was ended with 20 mL Na_2CO_3. Then was neutralized with 10% HCl solution (x3). The organic phase was purified by column chromatography on silica gel with 96:04, *n*-hexane-EtOAc, to afford **2f** (810 mg, 63.43 %). The structure of these compounds was established by NMR and mass data.

4.3. Synthesis of chalcones

The general procedure of the synthesis of chalcones is described in Scheme 1**.** Chalcones were prepared by Claisen-Schmidt condensation of benzaldehyde (**1**) and the alcoxyacetophenones (**2b-f**) in presence of KOH at reflux for 4 h. The reactions were monitoring by TLC and purified by column chromatography (*n*-hexane/EtOAc, 98:2) to give the respectively chalcones as yellow crystals (11.6 to 86.8 % yield). The halogenated chalcones **3g-j** were synthesized by allylic-halogenation using NBS and NIS with hν light radiation. **3k** was obtained by catalytic hydrogenation with Pd/C in CH_2Cl_2 at room temperature for 16 h. The new chalcone derivatives (**3h-3j**) were characterized by ^{1}H, ^{13}C NMR and mass spectra analysis.

*4.3.1. 2′-hydroxy-4′-methoxy-chalcone (**3b**)*

A solution of 2′-hydroxy-4′-methoxy acetophenone (**2b**) (600 mg, 3.6 mmol), benzaldehyde (0.44 mL mL, 4.32 mmol) and KOH (304.21.mg, 5.4 mmol) in MeOH, was heated at reflux for 4 h, it was monitoring by TLC and purified by column chromatography (*n*-hexane/EtOAc, 98:2) to afford **3b** as yellow crystals (790 mg, 86.8 % yield) M.p. 95-97 °C. EIMS, m/z: 254.09 $[M]^+$. NMR data were in good accordance with the literature.[33]

*4.3.2. 2′-hydroxy-4′-ethoxy-chalcone (**3c**)*

Chalcone **3c** was prepared from **2c** in a similar manner to the described for compound **3b**. EIMS, *m/z*: 268 $[M]^+$. NMR data were in good accordance with the literature.[34]

*4.3.3 2′-hydroxy-4′-propoxy-chalcone (**3d**)*

Chalcone **3d** was prepared from **2d** in a similar manner to the described for compound **3b.** EIMS, *m/z*: 282 $[M]^+$. NMR data were in good accordance with the literature.[35]

*4.3.4. 2′-hydroxy-4′-benzyloxy-chalcone (**3e**)*

Chalcone **3e** was prepared from **2e** in a similar manner to the described for compound **3b.** EIMS, *m/z*: 330 $[M]^+$. NMR data were in good accordance with the literature.[36]

*4.3.5. 2′-hydroxy-4′-acetoxy-chalcone (**3f**)*

Chalcone **3f** was prepared from **2f** in a similar manner to the described for compound **3b.** EIMS, *m/z*: 282 $[M]^+$. NMR data were in good accordance with the literature.[37]

*4.3.6. 2′-hydroxy-3′-iodine-4′-methoxy chalcone (**3g**) and 2′-hydroxy-4′-methoxy-5′-iodine-chalcone (**3h**)*

A mixture of 2′-hydroxy-4′-methoxy chalcone (**3b**) (100 mg, 0.4 mmol) and NIS (88.5 mg, 0.4 mmol) in chloroform was stirred and exposed to hν light for 60 min; affording a mixture of two compounds which were purified by column chromatography (*n*-hexane/EtOAc, 98:2→ 70:30), to obtain chalcones **3g** and **3h**.

*4.3.6.1. 2′-hydroxy-3′-iodine-4′-methoxy chalcone (**3g**).* Yellow crystals (52.3 mg, 22.9 %); mp 140-142 ºC; ^{1}H NMR (400 MHz, $CDCl_3$) δ: 14.26 (*s*, OH-2′), 7.93 (1H, d, *J* = 9.6 Hz, H-6′), 7.92 (1H, d, *J* = 15.6 Hz, H-β), 7.65-7.43 (5H, *m*, H-2-H-6), 7.58 (1H, d, *J* = 16 Hz, H-α), 6.55 (1H, d, *J* = 9.2 Hz, H-5′), 3.99 (3H, *s*, H-1′′); ^{13}C NMR (100 MHz, $CDCl_3$) δ: 191.80 (C-7), 164.83 (C-4), 164.78 (C-2′′), 145.70 (C-β), 134.75 (C-6′), 131.95 (C- 1), 131.16 (C-4), 129.26 (C-3, 5), 128.86 (C-2, 6), 119.77 (C-α), 115.13 (C-1′), 102.61 (C-3′, C-5′), 57.01 (C-1′′); EIMS, m/z: 380 $[M]^+$.Anal. calcd for $C_{16}H_{13}IO_3$: C, 50.55; H, 3.45; I, 33.38. Found: C, 49.80; H, 3.40; I, 32.36.

*4.3.6.2. 2′-hydroxy-4′-methoxy-5′-iodine-chalcone (**3h**).* Yellow crystals (73.5 mg, 32.2%); mp 130-132°C; ^{1}H NMR (400 MHz, $CDCl_3$) δ: 13.41 (1H, s, OH-2′), 8.25 (1H, s, H-6′), 7.90 (1H, d, *J* = 15.2 Hz, H-β), 7.68-7.44 (5H, m, H-2-H-6), 7.51 (1H, d, *J* = 15.2 Hz, H-α), 6.46 (1H, s, H-3′), 3.92 (3H, *s*, H-1′′); ^{13}C NMR (100 MHz, $CDCl_3$) δ: 191.22 (C-7), 166.95 (C-4′), 164.07 (C-2′), 145.59 (C-β), 140.24 (C-6′), 134.73 (C-1), 131.18 (C-4), 129.24 (C-3, C-5), 128.94 (C-2, C-6), 119.88 (C-α), 116.38 (C-1′), 100.48 (C-3′), 73.55 (C-5′), 56.95 (C-1′′). EIMS, m/z: 380 $[M]^+$. Anal. calcd for $C_{16}H_{13}IO_3$: C, 50.55; H, 3.45; I, 33.38. Found: C, 49.78; H, 3.40; I, 32.25.

*4.3.7. Synthesis of 2′-hydroxy-4′-methoxy-3′-bromo-chalcone (**3i**) and 2′-hydroxy-4′-methoxy-5′-bromo-chalcone (**3j**)*

A mixture of 2′-hydroxy-4′-methoxy chalcone (**3b**) (100 mg, 0.4 mmol) and NBS (70.07 mg, 0.4 mmol) in chloroform was stirred and exposed to hν light for 60 min; afforded a mixture of two compounds and were purified by column chromatography (*n*-hexane/EtOAc, 98:2→ 70:30), to obtain a mixture of **3i** and **3j** (74.9 mg, 37.45%) m.p. 170-172°C. **3j** spectroscopy data was in good accordance with litarature.[38] The structure of **3i** was established by NMR and mass data.

*4.3.7.1. 2′-hydroxy-4′-methoxy-3′-bromo-chalcone (**3i**)*. Yellow crystals (23.3 mg, 11.6%); m.p. 158-160°C; ^{1}H NMR (400 MHz, $CDCl_3$) δ: 14.01 (1H, s, OH-2′), 7.93 (1H, d, *J* = 15.2 Hz, H-β), 7.91 (1H, d, *J* = 9.2 Hz, H-6′), 7.66-7.44 (5H, m, H-2-H-6), 7.58 (1H, d, *J* = 15.2 Hz, H-α), 6.55 (1H, d, *J* = 9.2 Hz, H-5′), 4.00 (1H, s, H-1′′); ^{13}C NMR (100 MHz, $CDCl_3$) δ: 191.42 (C- 7), 166.00 (C-2′), 162.09 (C-4′), 145.64 (C-β), 134.70 (C-6′), 133.87 (C-1), 131.19 (C-4), 129.26 (C-3, 5), 128.94 (C-2, 6), 119.85 (C-α), 115.08 (C-1′), 101.45 (C- 5′), 101.24 (C-3′), 56.82 (C-1′′). EIMS, m/z: 332 $[M]^+$. Anal. calcd for $C_{16}H_{13}BrO_3$: C, 57.68; H, 3.93; Br, 23.98. Found: C, 56.85; H, 3.97; Br, 24.02.

*4.3.8. Synthesis of 2′-hydroxy-4′-methoxydihydro-chalcone (**3k**)*

2′-hydroxy-4′-methoxydihydro-chalcone (**3k**) was obtained from **3b** (200 mg, 0.78 mmol) by catalytic hydrogenation with Pd/C (20 mg) in CH_2Cl_2 (10 mL) and stirred at room temperature for 16 h. It was monitoring by TLC and purified by column chromatography (*n*-hexane/EtOAc, 98:2→80:20) to give **3k** as white crystals (156 mg, 50.6 %) M.p. 95-97°C. EIMS, m/z: 256 $[M]^+$. NMR data were in good accordance with the literature.[39]

*4.3.9. Synthesis of 2′, 4′-dihydroxy chalcone (**3a**)*

A mixture of **3e** (50 mg, 0.15 mmol) in 3mL of anhydrous dichloromethane was stirred at -78°C for 15 min under nitrogen, then was slowly added BBr_3 (0.1 mL, 0.001 mmol) and stirred at -78°C for 30 min. After the time, the flask was cooled for 8 h and warmed under room temperature. Finally, the crude reaction was purified by column chromatography with 80:20 *n*-hexane-EtOAc. The product **3a** was obtained as a crystalline yellow solid (19 mg, 52%). NMR data were in good accordance with the literature.[40]

4.4. Biological Activity

4.4.1. Antiproliferative Activity

Chalcone derivatives **3a-3j**, were subjected to antiproliferative assays against PC-3 (prostate), MCF-7(breast), HF-6 (colon) and CaSki (cervical) human cancer cell lines, we also included human fibroblasts cell line (BJ) as a control of non-cancerous cells, obtained from ATCC (American Type Culture Collection, Manassas, VA, USA). PC3 and CaSKi cells were grown in RPMI-1640 medium (Sigma Aldrich, St. Louis, MO, USA), while MCF7 and KB in Eagle's Minimum Essential Medium, (Invitrogen, Thermo Fisher Scientific, Inc., Waltham, MA, USA) and supplemented with fetal bovine serum 10%

(SFB, Invitrogen) and with 2 mM glutamine, all cultures were incubated at 37°C in atmosphere of 5% CO_2 atmosphere.

8000 cells per well in 96-well plate were cultured for starting the cytotoxic evaluation. The chalcone derivatives were solubilized in DMSO, the concentrations used were 80, 8, 0.8, 0.08, and 0.008 µg/mL for a dose/response curve and incubated at 37°C in 5% CO_2 atmosphere for 48 hrs and podophyllotoxin (PDX) was used as positive control. For determining the number of viable cells in proliferation we used CellTiter 96® AQueous One Solution Cell Proliferation Assay kit (Promega, Madison, WI, USA), following the manufacturer's instructions. Cell viability was determined by absorbance at 450 nm using an automated ELISA reader. The experiments were conducted by triplicate in three independent experiments. Data were analyzed in Prism 5.0 statistical program and the IC_{50} were determined by regression analysis.

4.4.2. Cell Cycle Analysis.

PC3 cancer cells lines (2.0×10^5) were plated in 6-well plates and allowed to attach overnight at 37°C in 5% CO_2. Exponential growing cells were exposed to the chalcone derivatives in accordance with IC_{50} values for 48 h and compared to podophyllotoxin (PDX) (0.12 μM) which was used as the positive control of the G2/M phase arrest. Cells from each treatment were trypsinized and collected into single cell suspensions, centrifuged, and fixed in cold ethanol (70%) overnight at −20∘C. The cells were then treated with RNase (0.01M, Sigma Aldrich) and stained with propidium iodide (PI) (7.5 µg/mL, Invitrogen) for 30 min in the dark, PI has the ability to bind to DNA molecules, and then RNase was added in order to allow PI to bind directly to DNA. The percentage of cells in G1, S, and G2 phases was analyzed with a flow cytometer (Becton, Dickinson, FACS Calibur, San Jose, CA); the number of cells analyzed for each sample was 10,000. Data obtained from the flow cytometer were analyzed using the FlowJo Software (Tree Star, Inc., Ashland, OR, USA) to generate DNA content frequency histograms, and to quantify the number of cells in the individual cell cycle phases.

4.4.3. Cell Death

PC3 were cultured, 25000 cells per well in 24-well plates, and then were treated for 48 hours according to the IC_{50} of each compound in each cell line. Cells were treated 30 min with H_2O_2 for the apoptosis control death and for necrosis control the cells were

boiling in water at 95°C for 10 sec. After 48 hours of treatment the cells were exposed to a solution of acridine orange (AO) and ethidium bromide (EB) (100 µg/mL AO, 100 µg/mL EB), according to procedures reported.[41] The cells were observed using a fluorescence microscope, AO/EB are intercalating nucleic acids specific fluorochromes and when bounded to DNA they emitted green and orange fluorescence, respectively. It is well known that AO can pass through cell membranes, but EB cannot. Necrotic cells stain red but have a nuclear morphology resembling that of viable cells. Apoptotic cells appear green, and morphological changes such as formation of apoptotic bodies are observed. The criteria for identification are as follows: viable cells appear to have green nucleus with intact structure; early apoptosis cells exhibit a bright green nucleus showing condensation of chromatin; late apoptosis appears as dense orange areas of chromatin condensation; and orange intact nucleus depicts secondary necrosis.[42, 43]

4.4.4. RT-PCR

1.25×10^5 PC3 cells were plated and treated with chalcones **3a**-**3c** for 48 hrs, the RNA was isolated. The total RNA extraction was performed employing a Quick-RNA MiniPrep Kit (Zymo Research, Irvine, USA), following the manufacturer's instructions. RNA was quantified using NanoDrop® ND-1000 (Thermo Scientific), and the RNA content of the samples was normalized. The RT-PCR was performed using a One-Step RT-PCR Kit with Thermo-Start Taq (Thermo Scientific) following the manufacturer's instructions.

The primer sequences for Bcl-2 were 5'-CCC TCC AGA TAG CTC ATT-3', and 5'-CTAGAC AGACAA GGA AAG-3'. The Bax primer sequences were 5'-ATG GAC GGG TCC GGG GAG-3', and 5'-TCAGAAAACATGTCAGCTGCC-3'. The GAPDH primers were 5'-CAAGGTCATCCATGACAACTTTG-3' and 5'-GTCCACCACCCTGTTGCTGTAG-3'. All primers were synthesized by IDT-Integrated DNA Technologies, the reaction products of the samples were analyzed in 1.5 % agarose gel.

4.4.5. Caspases activity

8000 PC3 cells were plated and treated with chalcones **3a**-**3c**, after treatment the caspase 3/7 activity was determined using The Caspase-Glo® 3/7 Assay in a luminescent assay (Promega, cat. G811C). The manufacturer's instructions were following. The results were represented as relative units of luminescence and represented in graphs, the statistical

analysis was performed using the Prism 5.0 statistical program and the test performed was t-student considered significant at $p < 0.05$.

4.5. Computational Details

4.5.1. Conformational analysis and geometry optimization

A conformational analysis of all the chalcone derivatives by using the SYBIL force field was performe.[44] The minimum energy conformer was submitted to a geometry optimization, employing the PM3 semi-empirical method.[45] In order to obtain more reliable values of energy and geometry, the lowest-energy structures were further optimized, within the density functional theory (DFT) formalism. For all the calculations the B3LYP[46] hybrid functional and the 6-31G* basis set for H, C, O and Br atoms, and LACVP* pseudopotential and basis set for Y atom were employed.[47] In order to ensure that the structure correspond to a minimum on the potential energy surface, a harmonic frequency analysis was done. All these calculations were performed using SPARTAN'08.[48]

4.5.2. Molecular graphics calculation

4.5.2.1. LUMO Map

We were interested in analyzing which regions of the chalcone derivatives are most electron deficient, and hence most subject to nucleophilic attack. For this, the lowest-unoccupied molecular orbital (LUMO) is mapped onto an electron density isosurface of 0.002 electrons/au^3. So, the LUMO map of all the chalcone structures was obtained.

4.5.2.2. Local Ionization Potential Map

Also, to identify which sites may be susceptible to electrophilic attack. We obtained the local ionization potential was mapped onto an electron density isosurface of 0.002 electrons/au^3. Therefore, local ionization potential maps of all the chalcone derivatives were calculated. This type of surface reveals those regions from which electrons are most easily ionized.[49]

4.5.2.3. Chemical reactivity molecular descriptors

As a first step, we calculated the vertical electron affinity (A) and the vertical ionization potential (I) employing the finite difference approximation, as it is shown below:

$$A = E^0 - E^- \quad (2)$$

$$I = E^+ - E^0 \quad (3)$$

Where E^0 is the total energy of the optimized structure, E^- and E^+ are the total energy of the anionic and cationic structures, respectively.[50] With these results we obtained the global reactivity molecular descriptors: chemical hardness (η), softness (S), chemical potential (μ) and Electrophilicity (ω), using the following equations:

$$\eta = \frac{I - A}{2} \tag{4}$$

$$S = \frac{1}{\eta} \tag{5}$$

$$\mu = \frac{I + A}{2} \tag{6}$$

$$\omega = \frac{\mu^2}{2\eta} \tag{7}$$

Also, we determined the Fukui function, employing the simplification proposed by Yang *et al.*, where the Fukui function can be calculated in terms of the atomic charge. This is possible by assuming that the electronic density in atom R can be expressed with its atomic partial charge (q_R). Since the derivative of the density with respect to the number of electrons (N) is discontinue, we need to evaluate the Fukui function from the left (f_R^-) and from the right (f_R^+). f_R^+ corresponds to a nucleophilic attack (electron wining), and f_R^- corresponds to an electrophilic attack (electron losing). The calculations were carried out with the following equations:

$$f_R^+ = q_R(N+1) - q_R(N) \tag{8}$$

$$f_R^- = q_R(N) - q_R(N-1) \tag{9}$$

Where $q_R(N)$ is the partial charge of R atom in the neutral molecule, $q_R(N+1)$ and $q_R(N-1)$ are the partial charge of R atom in the molecule as anion and cation respectively.[51] Furthermore, with all these results, we obtained the local reactivity molecular descriptors of softness (s_R^+ and s_R^-) and Electrophilicity (ω_R), as it is shown below:

$$s_R^+ = S f_R^+ \tag{10}$$

$$s_R^- = S f_R^- \tag{11}$$

$$\omega_R = \omega f_R^+ \quad (12)$$

Where s_R^+, s_R^- and ω_R are the softness and Electrophilicity value of R.[52]

4.5.3. QSAR construction and validation

All the global and local chemical reactivity molecular descriptors used in this study are displayed in Table 4. Local chemical reactivity descriptors correspond to the atoms that are important form the anticancer activity of chalcones, according to the molecular graphics analysis.

Table 4. Molecular Descriptors used in this study.

Molecular Descriptors	Type
$I, A, \eta, S, \mu, \omega$	Global chemical reactivity
$f_O^+, f_{C8}^+, f_{C\alpha}^+, f_{C\beta}^+, f_{C5}^+, f_O^-, f_{C8}^-, f_{C\alpha}^-, f_{C\beta}^-, f_{C5}^-, s_O^+, s_{C8}^+, s_{C\alpha}^+, s_{C\beta}^+, s_{C5}^+, s_O^-, s_{C8}^-, s_{C\alpha}^-, s_{C\beta}^-, s_{C5}^-, \omega_O, \omega_{C8}, \omega_{C\alpha}, \omega_{C\beta}, \omega_{C5}$	Local chemical reactivity

Genetic algorithms technique (GA) was employed for the construction of the mathematical model, with in the MobyDigs 01 software.[53] Chemical reactivity molecular descriptors and the biological activity (IC_{50}), of the chalcone derivatives, were used as the independent variables (X) and the dependent variable (Y), respectively. To validate our QSAR model, we employed the coefficient of determination (R^2), cross-validated R^2 (Q^2), standard deviation (s) and Fisher test (F).[54]

Also, to make a more sophisticated validation we used the QUIK, Q^2_{ASYM} redundancy (R^P) and over-fitting (R^N) rules. The QUIK rule is based on the K multivariate correlation index that measures the total correlation of a set of variables. This rule is a parameter that allows the rejection of models with high descriptor collinearity, and is defined as:

$$K = \frac{\sum_j \left[\frac{\lambda_j}{\sum_j \lambda_j} - \frac{1}{p}\right]}{\frac{2(p-1)}{p}} \quad j = 1, \ldots, p \quad and \quad 0 \leq K \leq 1 \quad (13)$$

Where λ are the values obtained from the correlation matrix of the data set $\mathbf{X}$ (n, p), n represents the number of molecules and p the number of descriptors. The total correlation

in the set given by the model descriptors X plus the response $Y(K_{XY})$ should always be greater than that measured only in the set of descriptors (K_X). Therefore, if $K_{XY} - K_X < \delta K$ the model is rejected, where δK has values of 0.01 to 0.05; models with negative differences are unacceptable.

The goal of the REDUNDANCY rule is to detect models with an excess of good molecular descriptors (R^P) and establishes that if $R^P < t^P$ the model is rejected. Depending on the data,t^P values range from 0.01 to 0.1. R^P is defined by:

$$R^P = \prod_{j=1}^{P^+} \left(1 - Mj\left(\frac{p}{p-1}\right)\right) Mj > 0 \text{ and } 0 \leq R^N \leq 1 \qquad (14)$$

On the other hand, the purpose of the OVERFITTING rule is to detect models with an excess of bad molecular descriptors. This rule stipulates that if $R^N < t^N(\varepsilon)$ the model is rejected. The $t^N(\varepsilon)$ values are calculated by:

$$t^N(\varepsilon) = \frac{p.\varepsilon - R}{p.R} \qquad (15)$$

Where ε values range from 0.01 to 0.1 and p is the number of variables in the model. R^N is defined by:

$$R^N = \sum_{j=1}^{P^-} Mj \qquad Mj < 0 \text{ and } -1 < R^N \leq 0 \qquad (16)$$

Where Mj is defined by:

$$Mj = \frac{R_{jY}}{R} - \frac{1}{P} \quad -\frac{1}{P} \leq Mj \leq \frac{P-1}{P} \qquad (17)$$

R_{jY} is the absolute value of the regression coefficient between the *jth* descriptors and the response Y. Additionally, we evaluated the predictive ability of our model by the Leave-One-Out (Q^2_{LOO}) method and the asymptotic squared Q rule (Q^2_{ASYM}).

In the Q^2_{LOO} method one compound is removed from the data set and the activity (Y_{Exp}) is correlated using the rest of the data set. The equation to calculate Q^2_{LOO} is:

$$Q^2_{LOO} = 1 - \frac{\sum_{i=1}^{n}\left(\hat{y}_{\overline{i}} - y_i\right)^2}{\sum_{i=1}^{n}(y_i - \bar{y})^2} \qquad (18)$$

Where $\hat{y}_{i/i}$ is the predicted value of the activity (Y_{Pred})

The asymptotic squared Q rule (Q^2_{ASYM}) establishes that a model is predictive if $Q^2_{LOO} - Q^2_{ASYM} > \delta Q$, and δQ values range from -0.005 to 0.005. The equation that defines Q^2_{ASYM} is:

$$Q^2_{ASYM} = 1 - (1 - R^2)\left(\frac{n}{n - p'}\right)^2 \quad (19)$$

Where n is the number of molecules and p' the number of molecular descriptors in the model.[48]

Applicability domain evaluation was carried out by means of the William plot construction, which depends in the leverage values and the standardized error in calculation. The leverage values (h) are obtained from the leverage matrix $\boldsymbol{H}$ which contains information about the descriptors on which the model is built. The leverage matrix $\boldsymbol{H}$ is defined as:

$$\boldsymbol{H} = \boldsymbol{X}.(\boldsymbol{X}^T.\boldsymbol{X})^{-1}.\boldsymbol{X}^T \quad (20)$$

Where $\boldsymbol{X}$ is the selected descriptor matrix; $\boldsymbol{X}^T$ is the transpose matrix of $\boldsymbol{X}$; and $(\boldsymbol{X}^T.\boldsymbol{X})^{-1}$ is the inverse of matrix $(\boldsymbol{X}^T.\boldsymbol{X})$. The leverage values are the diagonal elements of the H matrix. The warning leverage (h^*) is calculated as $h^* = 3p/n$, where n is the number of molecules and p is the number of descriptors in the model plus one. If one of the compounds has a leverage value higher than the h^* is will be considered an outlier, this is, out of the applicability domain of the model.[55]

Acknowledgments

The authors are thankful for the financial support from CONACyT (Grant CB 240801). RSRH thanks CONACyT for its "Retention" scholarship (C-291229-UAEMOR MOD.ORD./54/2017). The authors thank Laboratorio Nacional de Estructura de Macromoléculas (Conacyt 292696 and 294406) for the spectroscopic and mass analyses. We also thank Laboratorio de Dinámica de Proteínas and the LANCAD for the computing resources used in this work.

References

1. Veitch NC, Grayer RJ. Chalcones, Dihydrochalcones, and Aurones. In Flavonoids. Chemistry, Biochemistry and Applications. Andersen ØM, Markham KR, eds. CRC Press. 2005:1003–1100.
2. Yadav VR, Prasad S, Sung B, Aggarwal BB. The role of chalcones in suppression of NF-κB-mediated inflammation and cancer. *Int Immunopharmacology*. 2011;11:295–309.
3. Yadav JR, Elias DW, Beazely MA, Kandepu NM. Bioactivities of chalcones. C*urr Med Chem*. 1999;6:1125-1149.
4. Das M, Manna K. Chalcone Scaffold in Anticancer Armamentarium: A Molecular Insight. *J Toxicol*. 2016:1–4.
5. Zhang EH, Wang RF, Guo SZ, Liu B. An Update on Antitumor Activity of Naturally Occurring Chalcones. *Evid.-Based Complementary Altern. Med.* 2013:81562.
6. Batovska DI, Todorova IT. Trends in Utilization of the Pharmacological Potential of Chalcones. *Curr Clin Pharmacol*. 2010;5:1-29.
7. Singh P, Anand A, Kumar V. Recent developments in biological activities of chalcones. A mini review. *Eur J Med Chem.* 2014:85, 758-777.
8. Chen WH, Wang R, Shi YP. Flavonoids in the Poisonous Plant *Oxytropis falcate*. *J Nat Prod.* 2010;73:1398–1403.
9. Ghani NA, Ahmat N, Ismail NH, Zakaria I, Zawawi NK. Chemical constituents and cytotoxic activity of *Polyalthia cauliflora* var. *cauliflora*. *Res J Med Plant*. 2012;6:74–82.
10. Talia JM, Tonn CE, Debattista NB, Pappano. Antibacterial efficacy of dihydroxylated chalcones in binary and ternary combinations with nalidixic acid and nalidixic acid-rutin against *Escherichia coli* ATCC 25922. *Indian J Microbiol*. 2012;52:638–641.
11. Zampini IC, Villarini M, Moretti M, Dominici L, Isla MI. Evaluation of genotoxic and antigenotoxic effects of hydroalcoholic extracts of *Zuccagnia punctata* Cav. *J Ethnopharmacol*. 2008;115:330–335.

12. Iwata S, Nishino T, Nagata N, Satomi Y, Nishino H, Shibata S. Anti-tumorigenic activities of chalcones. I. Inhibitory effects of chalcone derivatives on Pi-incorporation into phospholipids of HeLa cells promoted by 12-O-tetradecanoyl-phorbol 13-acetate (TPA). *Biol Pharm Bull*. 1995;18:1710–1713.
13. Kupcewicz B, Jarze AA, Małecka M, Krajewska U, Rozalski M. Cytotoxic activity of substituted chalcones in terms of molecular electronic properties. *Bioorg Med Chem Lett*. 2014;24:4260–4265.
14. Lou C, Yang G, Cai H, Zou M, Xu Z, Li Y, Zhao F, Li W, Tong L, Wang M, Cai B. 2',4'-Dihydroxychalcone-induced apoptosis of human gastric cancer MGC-803 cells via downregulation of surviving mRNA. *Toxicol In Vitro*. 2010;24:1333–1337.
15. Sánchez-Picó A, León-González AJ, Martín-Cordero C, Daga RR. "Screening for natural anticancer agents using a fission yeast bioassay. *Phytochem Lett.* 2014;8:184–189.
16. Haddad AQ, Venkateswaran V, Viswanathan L, Teahan SJ, Fleshner NE, Klotz LH. Novel antiproliferative flavonoids induce cell cycle arrest in human prostate cancer cell lines. *Prostate Cancer Prostatic Dis* 2006;9:68–76.
17. Perro MP, Cravo S, Lima RT, Vasconcelos MH, Nascimento MS, Silva AM, Pinto S, Cidade M, Corrêa AG. Solid-phase synthesis of 20-hydroxychalcones. Effects on cell growth inhibition, cell cycle and apoptosis of human tumor cell lines. *Bioorg. Med. Chem.* 2012;20:25–33.
18. Arianingrum R, Sunarminingsih R, Meiyanto E, Mubarika S. Potential of a Chalcone Derivate Compound as Cancer Chemoprevention in Breast Cancer. *Int Conference Chem Chemical Eng*. 2012;38:41–45.
19. Wu W, Ye H, Wan L, Han X, Wang G, Hu J, Tang M, Duan X, Fan Y, He S, Huang L, Pei H, Wang X, Li X, Xie C, Zhang R, Yuan Z, Mao Y, Wei Y, Chen L. Millepachine, a novel chalcone, induces G2/M arrest by inhibiting CDK1 activity and causing apoptosis via ROS-mitochondrial apoptotic pathway in human hepatocarcinoma cells in vitro and *in vivo*. *Carcinogenesis* 2013;34:605–611.
20. Pilatova M, Varinska L, Perjesi P, Sarissky M, Mirossay L, Solar P, Ostro A, Mojzis J. *In vitro* antiproliferative and antiangiogenic effects of synthetic chalcone analogues. *Toxicol. In vitro*. 2010;24:1347–1355.

21. Rozmer Z, Berki T, Perjési P. Different effects of two cyclic chalcone analogues on cell cycle of Jurkat T cells *Toxicol. In Vitro*, 2006;20:1354–1362.
22. Romagnoli R, Baraldi PG, Carrion MD, Lopez Cara C, Cruz-Lopez O, Preti D, Tolomeo M, Grimaudo S, DiCristina A, Zonta N, Balzarini J, Brancale A, Sarkar T, Hamel E. Design, synthesis, and biological evaluation of thiophene analogues of chalcones. *Bioorg. Med. Chem*. 2008;16:5367–5376.
23. Liu X, Go ML, Antiproliferative properties of piperidinylchalcones, *Bioorg. Med. Chem.* 2006;14:153–163.
24. Rao YK, Fang SH, Tzeng YM. Differential effects of synthesized 20-oxygenated chalcone derivatives: modulation of human cell cycle phase distribution, *Bioorg. Med. Chem*. 2004;12:2679–2686.
25. Penninger JM. Kroemer G. Mitochondria, AIF and caspases–rivaling for cell death execution. *Nat. Cell Biol*. 2003;5:97–99.
26. Isa NM, Abdul AB, Abdelwahab SI. Abdullah R, Sukari MA, Kamalidehghan B, Hadi AH, Mohan S. Boesenbergin A. A chalcone from *Boesenbergia rotunda* induces apoptosis via mitochondrial dysregulation and cytochrome c release in A549 cells *in vitro*: involvement of HSP70 and Bcl2/Bax signaling pathways *Journal of Functional Foods* 2013;5:87-97.
27. Naseri MH, Mahdavi M, Davoodi J, Tackallou SH, Goudarzvand M, Neishabouri SH. Up regulation of Bax and down regulation of Bcl2 during 3-NC mediated apoptosis in human cancer cells. *Cancer Cell Int*. 2015;15:55; doi 10.1186/s12935-015-0204-2.
28. Green DR, Reed JC. Mitochondria and apoptosis. *Scienc*e. 1998;281:1309–1312.
29. Antonsson B. Conti F, Ciavatta A, Montessuit S, Lewis S, Martinou I, Bernasconi L, Bernard A, Mermod JJ, Mazzei G, Maundrell K, Gambale F, Sadoul R, Martinou JC. Inhibition of Bax channel-forming activity by Bcl-2. *Science.* 1997;277:370–372.
30. Romagnoli R, Baraldi PG, Carrion MD, Cruz-Lopez O, Cara CL, Balzarini J, Hamel E, Canella A, Fabbri E, Gambari R, Basso G, Viola G. Hybrid α-bromoacryloylamidochalcones. Design, synthesis and biological evaluation. *Bioorg. Med. Chem. Lett*. 2009;19:2022–2028.

31. Fortuna CG, Barresi V, Musumarra G. Design, synthesis and biological evaluation of trans 2-(thiophen-2-yl)vinyl heteroaromatic iodides. *Bioorg. Med. Chem.* 2010;18:4516-4523.
32. Fortuna CG, Barresi V, Berellini G, Musumarra G. Design and synthesis of trans 2-(furan-2-yl)vinyl heteroaromatic iodides with antitumour activity. *Bioorg. Med. Chem.* 2008; 16:4150-4159.
33. Nguyen MT, Tran Thi C, Nguyen VV, Nguyen VT. Study on transformation of some α, β-unsaturated ketones from 2-hydroxy-4-methoxyacetophenone. *Tap Chi Hoa Hoc*. 2008;46:470–474.
34. Joshi RS, Naik HB. Chalcones derived from 2-hydroxy-4-ethoxyacetophenone. *J Institution Chemists (India)*. 1978;50(4):153–155.
35. Desai B, Modi S, Naik HB. Studies on pyrazolines - Part-I: Preparation and antibacterial activity of 1-H-3-(2'-hydroxy-4'-n-propoxyphen-1'-yl)-5-substituted phenyl-2-pyrazolines *J Indian Council Chem*. 1994;10:1-3.
36. Saiyad IZ, Nadkarni DR, Wheeler TS. Chalcones. The condensation of aromatic aldehydes with resacetophenone. *J Chem Society*. 1937;1737–1739.
37. Narender T, Papi K, Kumar B. BF_3OEt_2 mediated regioselective deacetylation of polyacetoxyacetophenones and its application in the synthesis of natural products. *Tetrahedron Lett.* 2008;49:4409–4415.
38. Barot V, Modi M, Naik HB. New 5-(2-hydroxy-4-methoxy-5-bromophenyl)-7-(substituted phenyl)-2,3,6,7 tetrahydro-1,4-oxazepines. *J Institution Chemists (India)*. 1999;71:70–71.
39. Xiaojing Z, LingyuL, Norbo K. Flevnoids from Tibetan medicine *Oxytropis falcate* Bunge. *J Chinese Pharma Science.* 2014;23:99–105.
40. Benabderahmane W, Mezrag A, Bouheroum M, Benayache F, Mosset P. The chemical investigation of the chloroformic extract of *Ononis angustissima* Lam. Var. species. *Der Pharmacia Lettre*. 2014;6:88–91.
41. Sánchez-Carranza JN, Alvarez L, Marquina-Bahena S, Salas-Vidal E, Cuevas V, Jiménez EW, Veloz GRA, Carraza M, González-Maya L. Phenolic Compounds Isolated from *Caesalpinia coriaria* Induce S and G2/M Phase Cell Cycle Arrest

Differentially and Trigger Cell Death by Interfering with Microtubule Dynamics in Cancer Cell Lines. *Molecules.* 2017;22:666

42. Kasibhatla S, Amarante-Mendes GP, Finucane D, Brunner T, Bossy-Wetzel E, Green DR. Acridine orange/ethidium bromide (AO/EB) staining to detect apoptosis. *Cold Spring Harb. Protoc*. 2006, 3, pdb-prot4493.
43. Mohan S, Bustamam A, Ibrahim S, Al-Zubairi AS, Aspollah M, Abdullah R, Elhassan MM. *In vitro* ultramorphological assessment of apoptosis on CEMss induced by linoleic acid-rich fraction from *Typhonium flagelliforme* tuber. *Evid. Based Complement. Altern Med*. 2011:421894.
44. Clark M, Cramer III RD, Opdensch van N. Validation of the general purpose tripos 5.2 force field. *J Computational Chem*. 1989;10:982.
45. Stewart JJ. Optimization of parameters for semiempirical methods I. Method. *J Comput Chem.* 1989;10, 209–220.
46. Stephens PJ, Devlin F, Chabalowski CF, Frisch MJ. Ab Initio Calculation of Vibrational Absorption and Circular Dichroism Spectra Using Density Functional Force Fields. *J Phys Chem*. 1994;45:11623–11627.
47. Hay PJ, Wadt WR. Ab initio effective core potentials for molecular calculations. Potentials for main group elements Na to Bi. *J Chem Phys*. 1985;82:299; doi.org/10.1063/1.448975.
48. Wavefunction, Inc. Spartan'08. Available from www.wavefun.com. Accessed 30 Dec. 2015.
49. Abdel-Mottaleb MSA. DFT Studies of Caffeic Acid Antioxidant: Molecular Orbitals and Composite Reactivity Maps Correlation with Photophysical Characteristics and Photochemical Stability. *J Chem*. 2016:1–8.
50. Razo-Hernández RS, Pineda-Urbina K, Velazco-Medel MA, Villanueva-García M, Sumaya-Martínez MT, Martínez-Martínez J, Gómez-Sandoval Z. QSAR study of the DPPH· radical scavenging activity of coumarin derivatives and xanthine oxidase inhibition by molecular docking. *Cent Eur J Chem.* 2014;12:1067–1080.
51. Morales-Bayuelo A, Caballero J. New insights into steric and electronic effects in a series of phosphine ligands from the perspective of local quantum similarity using the Fukui function. *J Mol Modelling*. 2015:2–11.

52. Roy DR, Parthasarathi R, Subramanian V, Chattaraj PK. An Electrophilicity Based Analysis of Toxicity of Aromatic Compounds Towards Tetrahymena Pyriformis. *QSAR Combinatorial. Science*. 2006;2:114–122.
53. Todeschini R, Consonni V, Mauri A, Pavan M. Detecting "bad" regression models: multicriteria fitness functions in regression analysis *Anal Chim Acta.* 2004;515,199–208.
54. Pérez D, Sarabia O, Villanueva-García M, Pineda-Urbina K, Ramos-Organillo A, Gonzalez-Gonzalez J, Gomez-Sandoval Z, Razo-Hernández RS. *In silico* receptor-based drug design of X, Y- benzenesulfonamide derivatives as selective COX-2 inhibitors, *Comptes Rendus Chimie*. 2017;20,169–180.
55. Song-Bing H, Ben H, Zheng-Kun K, Dong W, De-Xin K. Predicting Subtype Selectivity for Adenosine Receptor Ligands with Three-Dimensional Biologically Relevant Spectrum (BRS-3D), SCIENTIFIC REPORTS. 2016; 6, 36595.

Figure Legends

Fig. 1. Effect of chalcones on cell cycle in PC3 cell line of prostate cancer. A) Negative Control; B) 3a; C) 3b; D) 3c; E) Podophyllotoxin (positive control).

Fig. 2. Effect of chalcones on cell death by epifluorescence microscopy in PC3 cell line of prostate cancer. A) andB) Negative Controls; C) **3a**; D) **3b**; E) **3c**; F) H_2O_2 apoptosis positive control; G) Podophyllotoxin 0.005 µM apoptosis positive control; H) Necrosis control.

Fig. 3. Effect of **3a**, **3b** and **3c**, on mRNA expression levels of Bcl-2 and Bax in PC3 cells after 48 hours treatment. GAPDH was used as an internal control.

Fig. 4. Caspase 3/7 activity for treatment of **3a**, **3b**, **3c**, and paclitaxel (TX) in PC3 cells. *p<0.05, **p<0.01, ***p<0.001 compared with the control group.

Fig. 5. LUMO map of all the chalcone derivatives (**3a**-**3k**). Blue, green, yellow and red colors indicate the most, medium, poor and none populated region of the LUMO orbital, respectively.

Fig. 6. Local ionization potential map of all the chalcone derivatives (**3a**-**3k**). Red, yellow, green and blue colors indicate zones from which electrons are most easily, medium, less and unlikely ionized, respectively.

Fig. 7. A) Linear relation of calculated activity versus experimental activity. B) Linear relation of predicted activity versus experimental activity.

Fig. 8. Williams plot of prediction residuals versus leverage values of chalcones. The horizontal line shows the warning leverage ($h^* = 3p/n$, n is the number of chalcones and p is the number of descriptors in the model plus one), the two vertical lines indicate the bounds within which all of residuals should lie (3SDEC=13.38).

Scheme Legends

Scheme 1. Synthesis of chalcones **3a-3k**.